frontiers in Energy Research

ORIGINAL RESEARCH
published: 25 August 2021
doi: 10.3389/fenrg.2021.732997

Design of Decentralized Adaptive Sliding Mode Controller for the Islanded AC Microgrid With Ring Topology

He Jiang[1,2]*, *Mofan Wei*[1,2], *Yan Zhao*[1,2] and *Ji Han*[1,2]

[1]School of Renewable Energy, Shenyang Institute of Engineering, Shenyang, China, [2]Key Laboratory of Regional Multi-energy System Integration and Control of Liaoning Province, Shenyang, China

Sliding mode control can restrain the perturbations generated from the intermittence of the renewable energy generation and the randomness of local loads when microgrids are operating in islanded mode. However, the microgrid consists of several subsystems and the interactions among them will cause the chattering problems under the overall sliding mode control. In this paper, the chattering restraint issues for voltage control of the islanded microgrid with a ring topology structure are investigated based on the decentralized adaptive sliding mode control strategies. Firstly, we construct a tracking error system with interconnections considering the power transmission among subsystems and nominal values of system states. Secondly, we design linear matrix inequalities (LMIs) according to the H_∞ attenuation performance of the system external disturbances. Then, the tracking error performance and the control precision are guaranteed via the asymptotic stabilities of integral sliding mode surfaces. Adaptive laws are utilized to address the chattering problems of the sliding mode control. Finally, simulation results verify the effectiveness of the proposed decentralized control methods.

Keywords: islanded microgrid, chattering restraint, voltage control, adaptive control, sliding mode control

OPEN ACCESS

Edited by:
Qiuye Sun,
Northeastern University, China

Reviewed by:
Wei Hu,
Zhejiang University, China
Jingwei Hu,
Northeastern University, China

***Correspondence:**
He Jiang
jianghescholar@163.com

Specialty section:
This article was submitted to Smart Grids, a section of the journal Frontiers in Energy Research

Received: *29 June 2021*
Accepted: *09 August 2021*
Published: *25 August 2021*

Citation:
Jiang H, Wei M, Zhao Y and Han J (2021) Design of Decentralized Adaptive Sliding Mode Controller for the Islanded AC Microgrid With Ring Topology. Front. Energy Res. 9:732997. doi: 10.3389/fenrg.2021.732997

INTRODUCTION

Recently, there are abundant distributed generating devices permeating in the modern electric power systems for achieving the environment protection and the effective and flexible control of grids. In order to ensure the extensiveness and security of the power supply, microgrids have been the main form to transmit electricity to local loads for remote regions, which can operate in islanded mode or grid-connected mode (Mahmoud et al., 2014). Actually, an AC islanded microgrid consisting of distributed generation units (DGus) and energy storage devices can supply power to local loads steadily in low voltage magnitude (Kabalan et al., 2017). Because the microgrid contains numerous power electronic facilities, such as voltage source converters (VSC) et al., it is lack of immense inertia provided by rotating devices comparing with conventional grids (Zou et al., 2019). Furthermore, the renewable generation devices are usually affected by weather conditions and the power generated from them is usually intermittent and uncertain, so it is more complicated to realize the stable control of the multi-area microgrid voltage when it is in islanded mode (Zhou et al., 2021). At present, there are different control strategies to solve the voltage control problems of multi-area microgrids and optimize the control performance in islanded mode in order to improve the reliability and effectiveness of the power supply (Divshali et al., 2012; Sahoo et al., 2018).

The conventional control methods for multi-area microgrids operating in islanded mode demonstrate several disadvantages. The close-loop proportional-integral-derivative (PID) voltage control strategy can not estimate the errors between state variables and the nominal sinusoidal voltages accurately. Additionally, this control strategy presents bad control performance for restraining the inner parameter perturbations, such as frequency fluctuations (Vandoorn et al., 2013; Chen et al., 2015; Sefa et al., 2015). Zeb et al. (2019) combined the PID control method with fuzzy principles and designed the proportional resonant harmonic compensator as a current controller. Moreover, a phase lock loop (PLL) was designed to promote the speed of the system dynamic response. A comparison between fuzzy sliding mode control (FSMC) and fuzzy PID control illustrated that the dynamic response speed was lower and the tracking error performance was less precise via the fuzzy PID method. Considering that microgrids are sensitive about the system parameter variations, so the droop control technology is proposed to improve the robustness of microgrids via simulating the droop relationships among different electrical parameters (Avelar et al., 2012; Beerten and Belmans, 2013; Eren et al., 2015; Wang et al., 2019; Wang et al., 2021). Mi et al. (2019) modified traditional linear droop control strategies and utilized nonlinear droop relationships to describe the interactions between reactive power and voltages. The T-S fuzzy theory was applied to approximate the nonlinear model accurately and coordinate power among each DGu. Nevertheless, there were also errors between stable values and nominal values of voltages. Recently, sliding mode control (SMC) strategies are extensively applied in the stability control of microgrids for the superior asymptotic stability and robustness against parameter uncertainties (Hu et al., 2010; Karimi et al., 2010; Liu et al., 2017). An integration model of microgrids with complex meshed topology structures and several DGus was constructed to achieve the power sharing and voltage robust control (Cucuzzella et al., 2017; Wang et al., 2020). But the integration model could not represent actual interaction effects in different subsystems and the chattering was serious. Mi et al. (2020) proposed an adaptive sliding mode control strategy based on the sliding mode observer for wind-diesel power systems. The microgrid bus voltage showed remarkable stability via regulating the reactive power in terms of this method. Contrarily, the disturbance observer and adaptive algorithm brought in numerous parameters and promoted the complexity of the control system. To figure out the problem of harmonic disturbance in microgrids, Esparza et al. (2017) proposed a comprehensive control strategy to restrain the harmonic currents generated from DGus in AC microgrids. As shown in the simulation results, this strategy could cause the chattering phenomenon inherently.

Motivated by the aforementioned discussions, for the multi-area microgrid with a ring topology, the decentralized voltage control model will represent more appropriate relationships among the parameters in each local subsystem comparing with the integrated one. In addition, the adaptive sliding mode control (ASMC) strategy, which will be designed according to H_∞ attenuation performance of each subsystem, can ensure the robustness of the interconnected systems against mismatched uncertainties and external perturbations.

The main contributions of this paper can be summarized as follows:

1) The established multi-area microgrid model can depict the interactions among subsystems appropriately;
2) The reliability of solutions and the attenuation performance of external disturbances can be ensured based on the linear matrix inequalities (LMIs);
3) The proposed decentralized ASMC can restrain the chattering of the microgrid.

The rest of research includes four sections. Section *Dynamical Models of Multi-Area Interconnected Microgrids* constructs state functions with interconnections representing the topology structure of microgrid systems and defines tracking error models based on the nominal values of the state variables. Section *Proposed Decentralized Adaptive Sliding Mode Voltage Controller* introduces the designed decentralized voltage controllers in terms of the proposed ASMC theory. Section *Simulation Results* provides the simulation results and Section *Conclusion* illustrates the conclusion.

DYNAMICAL MODELS OF MULTI-AREA INTERCONNECTED MICROGRIDS

In order to explain the power transmission among the multi-area microgrid, the electrical three-phase diagram of the ring topology system composed four DGus is shown in **Figure 1**. The researched microgrid consists of local loads, power transmission lines and DGus. Because of various energy storage components in renewable generation systems, the DGus could be represented as DC voltage sources. The DGus connect with the points of common coupling (PCC) via VSCs and filters and provide power to local loads. PCCs can also link one of areas of the microgrids to another and connect microgrids with main grids.

Considering the ring topology structure of the microgrid and the power transmission orientations among different areas, the voltage control model of subsystem i with interconnections in the dq-coordinates in terms of Kirchhoff's Curent Law (KCL) and Kirchhoff's Voltage Law (KVL) can be obtained as follows,

$$C_{ti}\dot{V}_{di} = \omega V_{qi} + I_{tdi} - I_{ldi} - I_{di} + \sum_{\substack{j\in N \\ j\neq i}} \xi_{ij} I_{dj} \tag{1}$$

$$C_{ti}\dot{V}_{qi} = -\omega V_{di} + I_{tqi} - I_{lqi} - I_{qi} + \sum_{\substack{j\in N \\ j\neq i}} \xi_{ij} I_{qj} \tag{2}$$

$$L_{ti}\dot{I}_{tdi} = -V_{di} - R_{ti} I_{tdi} + \omega L_{ti} I_{tqi} + U_{di} \tag{3}$$

$$L_{ti}\dot{I}_{tqi} = -V_{qi} - R_{ti} I_{tqi} - \omega L_{ti} I_{tdi} + U_{qi} \tag{4}$$

$$L_i\dot{I}_{di} = V_{di} - \sum_{\substack{j\in N \\ j\neq i}} \xi_{ij} V_{dj} - R_i I_{di} + \omega L_i I_{qi} \tag{5}$$

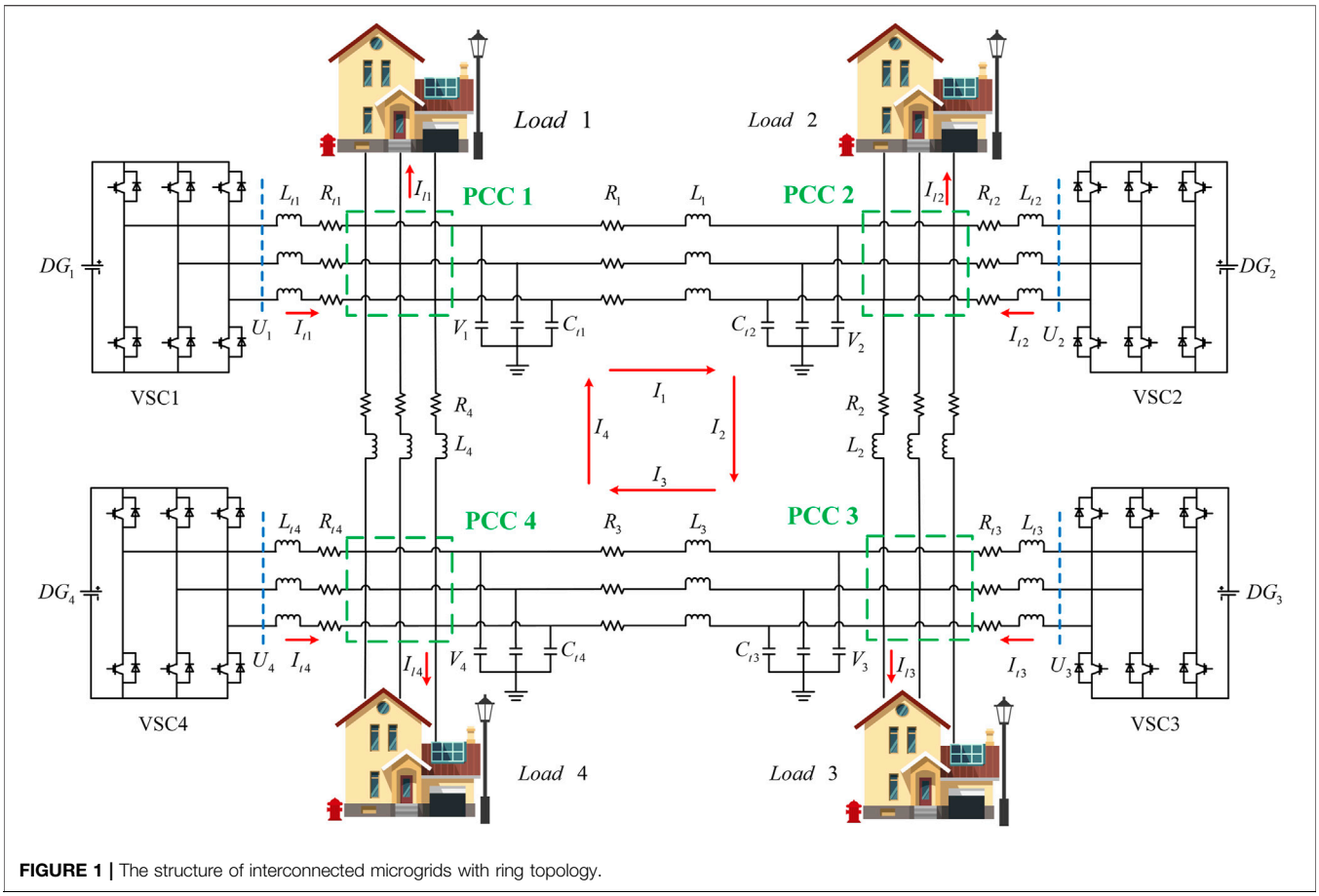

FIGURE 1 | The structure of interconnected microgrids with ring topology.

$$L_i\dot{I}_{qi} = V_{qi} - \sum_{\substack{j\in N \\ j\neq i}} \xi_{ij}V_{qj} - R_iI_{qi} - \omega L_iI_{di} \tag{6}$$

$$y_{1i} = V_{di} \tag{7}$$

$$y_{2i} = V_{qi} \tag{8}$$

where N is the number of DGus in microgrids, L_{ti}, C_{ti} and R_{ti} represent the inductance, capacitance and resistance of the filter connected with the DGu in subsystem i, respectively. The microgrid subsystems in various areas are integrated via interconnecting lines. L_i and R_i are the inductance and resistance of the interconnecting line between subsystem i and the adjacent subsystem. ξ_{ij} is the orientation of the interconnecting line current between subsystem i and subsystem j $(i \neq j)$. $\xi_{ij} = 1$ and $\xi_{ij} = -1$ represent the current flows into and flows out the subsystem i. However, $\xi_{ij} = 0$ represents there is no power exchange between subsystem i and subsystem j. V_{di} and V_{qi} are the direct and quadrature components of the PCC voltage in subsystem i. I_{di} and I_{qi} are the direct and quadrature components of interconnecting line i. I_{tdi}, I_{tqi}, U_{di} and U_{qi} are the direct and quadrature components of the current and voltage generated from DGu in subsystem i. I_{ldi} and I_{lqi} are the direct and quadrature components of local loads. The randomness of the local loads and the power generation intermittence of DGus will cause frequency fluctuation in microgrids. Therefore, we introduce the parameter uncertainties and donate system frequency $\omega = \omega_0 + \Delta\omega$. The matrix form of the dynamic **(1)**–**(8)** can be written as

$$\begin{cases} \dot{x}_i(t) = (A_i + \Delta A_i(t))x_i(t) + B_iu_i(t) + \sum\limits_{\substack{j\in N \\ j\neq i}} E_{ij}x_j(t) + F_id_i(t) \\ y_i(t) = C_ix_i(t) \end{cases} \tag{9}$$

where

$$A_i = \begin{bmatrix} 0 & \omega_0 & \frac{1}{C_{ti}} & 0 & -\frac{1}{C_{ti}} & 0 \\ -\omega_0 & 0 & 0 & \frac{1}{C_{ti}} & 0 & -\frac{1}{C_{ti}} \\ -\frac{1}{L_{ti}} & 0 & -\frac{R_{ti}}{L_{ti}} & \omega_0 & 0 & 0 \\ 0 & -\frac{1}{L_{ti}} & -\omega_0 & -\frac{R_{ti}}{L_{ti}} & 0 & 0 \\ \frac{1}{L_i} & 0 & 0 & 0 & -\frac{R_i}{L_i} & \omega_0 \\ 0 & \frac{1}{L_i} & 0 & 0 & -\omega_0 & -\frac{R_i}{L_i} \end{bmatrix};$$

$$\Delta A_i = \begin{bmatrix} 0 & \Delta\omega & 0 & 0 & 0 & 0 \\ -\Delta\omega & 0 & 0 & 0 & 0 & 0 \\ 0 & 0 & 0 & \Delta\omega & 0 & 0 \\ 0 & 0 & -\Delta\omega & 0 & 0 & 0 \\ 0 & 0 & 0 & 0 & 0 & \Delta\omega \\ 0 & 0 & 0 & 0 & -\Delta\omega & 0 \end{bmatrix};$$

$$E_{ij} = \begin{bmatrix} 0 & 0 & 0 & 0 & \frac{\xi_{ij}}{C_{ti}} & 0 \\ 0 & 0 & 0 & 0 & 0 & \frac{\xi_{ij}}{C_{ti}} \\ 0 & 0 & 0 & 0 & 0 & 0 \\ 0 & 0 & 0 & 0 & 0 & 0 \\ -\frac{\xi_{ij}}{L_i} & 0 & 0 & 0 & 0 & 0 \\ 0 & -\frac{\xi_{ij}}{L_i} & 0 & 0 & 0 & 0 \end{bmatrix};$$

$$B_i = \begin{bmatrix} 0 & 0 & \frac{1}{L_{ti}} & 0 & 0 & 0 \\ 0 & 0 & 0 & \frac{1}{L_{ti}} & 0 & 0 \end{bmatrix}^T;$$

$$F_i = \begin{bmatrix} -\frac{1}{C_{ti}} & 0 & 0 & 0 & 0 & 0 \\ 0 & -\frac{1}{C_{ti}} & 0 & 0 & 0 & 0 \end{bmatrix}^T;$$

where $x_i = [V_{di} V_{qi} I_{tdi} I_{tqi} I_{di} I_{qi}]^T \in \mathbb{R}^6$ is the state variable vector, $u_i = [U_{di} U_{qi}]^T \in \mathbb{R}^2$ is the control input vector, $d_i(t) = [I_{ldi} I_{lqi}]^T \in \mathbb{R}^2$ is the external disturbance vector and $y_i = [V_{di} V_{qi}]^T \in \mathbb{R}^2$ is the output vector. $A_i \in \mathbb{R}^{6\times6}$, $B_i \in \mathbb{R}^{6\times2}$ and $F_i \in \mathbb{R}^{6\times2}$ are the system matrix, control input matrix and the external disturbance matrix of the ith voltage control model of the microgrid. $\Delta A_i \in \mathbb{R}^{6\times6}$ is a time-varying matrix representing the frequency fluctuation and $E_{ij} \in \mathbb{R}^{6\times6}$ is the interconnection gain matrix consisting of ξ_{ij} and the parameters of interconnecting line i.

Assume that the nominal vector of the state vector in subsystem i is $x_i^* = [V_{di}^* V_{qi}^* I_{tdi}^* I_{tqi}^* I_{di}^* I_{qi}^*]^T$ and $\dot{x}_i^* = 0$. We define the error vector

$$e_i(t) = \begin{bmatrix} V_{di} - V_{di}^* \\ V_{qi} - V_{qi}^* \\ I_{tdi} - I_{tdi}^* \\ I_{tqi} - I_{tqi}^* \\ I_{di} - I_{di}^* \\ I_{qi} - I_{qi}^* \end{bmatrix} = x_i(t) - x_i^*. \tag{10}$$

In view of **(9)**, the corresponding error dynamic model in subsystem i can be expressed by

$$\dot{e}_i(t) = (A_i + \Delta A_i(t))e_i(t) + B_i u_i(t) + \sum_{\substack{j\in N \\ j\neq i}} E_{ij} e_j(t) + f_i(t) \tag{11}$$

where $f_i(t) \triangleq F_i d_i(t) + (A_i + \Delta A_i(t))x_i^* + \sum_{\substack{j\in N \\ j\neq i}} E_{ij} x_j^*$ represents the integration term of exogenous disturbance and parameter uncertainty based on nominal vector, which is Euclidean norm bounded by $\|f_i(t)\| \le \rho_i$, in which

$$\begin{aligned} \|f_i(t)\| &= \left\| F_i d_i(t) + (A_i + \Delta A_i(t))x_i^* + \sum_{\substack{j\in N \\ j\neq i}} E_{ij} x_j^* \right\| \\ &\le \|F_i\|\|d_i(t)\| + \|A_i x_i^*\| + \|a_i x_i^*\| + \left\| \sum_{\substack{j\in N \\ j\neq i}} E_{ij} x_j^* \right\| = \rho_i. \end{aligned} \tag{12}$$

For the later proof proceedings, we introduce the following lemmas, which can be needed to ensure the asymptotic stability of the system.

Lemma 1: (Mnasri and Gasmi, 2011) Consider the following unforced system:

$$\begin{cases} \dot{x} = Ax + H\omega \\ y = Cx \end{cases}$$

This system is regarded as quadratically stable and satisfies the H_∞ norm $\|T_{y\omega}\|_\infty < \gamma$. If there exists a quadratic Lyapunov function $V(x) = x^T P x$, with $P > 0$, then, for all $t > 0$,

$$\dot{V} + y^T y - \gamma^2 \omega^T \omega < 0$$

Lemma 2: (Mnasri and Gasmi, 2011) Let x and y be any vectors with appropriate dimensions. Then, for any scalar $\epsilon > 0$, the following inequality holds:

$$2x^T y \le \epsilon x^T x + \epsilon^{-1} y^T$$

Lemma 3: (Mnasri and Gasmi, 2011) Consider a partitioned symmetric matrix

$$\begin{bmatrix} A & B^T \\ B & C \end{bmatrix},$$

where A and C are square matrices with appropriate dimensions. Then, this matrix is negative define if and only if the matrix A and $C - BA^{-1}B^T$ are negative define.

PROPOSED DECENTRALIZED ADAPTIVE SLIDING MODE VOLTAGE CONTROLLER

The adaptive algorithm can optimize the parameters in controller and the decentralized strategy can improve the control performance. Design proceedings of sliding surface need to consider the stabilizing, tracking and restraining performance of the system. The sliding mode control law usually contains two parts, the switching control law and the equivalent control law. The former one can force the system state to approximate to the sliding surface when it deviates from the surface and the latter one can ensure the system state to keep on the sliding surface when it reaches on the surface.

In order to design decentralized adaptive sliding mode voltage control laws for error dynamic model **(11)**, the following assumptions are introduced.

Assumption 1: All the parameter uncertainty matrices caused by frequency fluctuations are viewed as bounded. That means

$$\|\Delta A_i(t)\| \le a_i. \tag{13}$$

Assumption 2: For each subsystem i,

$$\sum_{j=1, j\neq i}^{N} E_{ji}^T E_{ji} > 0. \tag{14}$$

For improving the dynamic response performance, we define the following integral sliding mode surface as

$$s_i(t) = H_i e_i(t) - \int_0^t H_i[(A_i - B_i K_i) e_i(\tau)] d\tau. \tag{15}$$

where $H_i \in \mathbb{R}^{2\times 6}$ is a constant matrix satisfying $H_i B_i$ is non-singular and $H_i B_i$ is positive for all $i \in N$. $K_i \in \mathbb{R}^{2\times 6}$ is the feedback matrix to be obtained via solving LMIs.

Substituting **Equation 11** into the derivative of sliding surface **(15)** yields

$$\dot{s}_i(t) = H_i \left[(\Delta A_i(t) + B_i K_i) e_i(t) + B_i u_i(t) + \sum_{\substack{j\in N \\ j\neq i}} E_{ij} e_j(t) + f_i(t) \right]. \tag{16}$$

When the state trajectory of the tracking error system arrive and keep on the sliding mode surface, it would satisfy the following equation.

$$s_i(t) = 0 \text{ and } \dot{s}_i(t) = 0 \tag{17}$$

Based on **Equation 17**, equivalent control law can be represented as

$$u_{ieq}(t) = -K_i e_i(t) - (H_i B_i)^{-1} H_i \left[\Delta A_i(t) e_i(t) + \sum_{\substack{j\in N \\ j\neq i}} E_{ij} e_j(t) + f_i(t) \right]. \tag{18}$$

Substituting **Equation (18)** into **(11)**, the sliding mode dynamic equation can further be expressed as

$$\dot{e}_i(t) = \left(A_i - B_i K_i + \widetilde{B}_i \Delta A_i(t)\right) e_i(t) + \widetilde{B}_i \sum_{\substack{j\in N \\ j\neq i}} E_{ij} e_j(t) + \widetilde{B}_i f_i(t) \tag{19}$$

where $\widetilde{B}_i = I - B_i (H_i B_i)^{-1} H_i$. **Equation 19** shows a more complicated tracking error system with parameter uncertainties and external disturbances. In the following procedures, we utilize the Lyapunov theory to analysis the system stability and the tracking performance to the nominal values of currents and voltages in each subsystem. Furthermore, we consider the H_∞ disturbance attenuation performance of interconnected system and design LMIs in terms of an H_∞ norm γ_i.

Theorem 1: Assume that the tracking error system **(19)** satisfies Assumption 1 and Assumption 2. If there exists a feasible solution $X_i > 0$, and R_i satisfies the following LMI **(20)**, then we consider uncertain system **(19)** matches the H_∞ condition.

$$\begin{bmatrix} \Omega_i & \widetilde{B}_i \widetilde{E}_i & \widetilde{B}_i & X_i C_i^T & a_i b_i X_i & X_i \\ * & -I & 0 & 0 & 0 & 0 \\ * & * & -\gamma_i^2 I & 0 & 0 & 0 \\ * & * & * & -I & 0 & 0 \\ * & * & * & * & -\varepsilon_1^{-1} I & 0 \\ * & * & * & * & -\omega_0 & -E_i^{-1} \end{bmatrix} < 0 \tag{20}$$

where $\Omega_i = X_i A_i^T + A_i X_i - B_i R_i - R_i^T B_i^T + \varepsilon_i I$ and $\varepsilon_i > 0$ is a positive scalar. We consider the sliding mode surface

$$s_i(t) = H_i e_i(t) - \int_0^t H_i \left[\left(A_i - B_i R_i X_i^{-1}\right) e_i(\tau) \right] d\tau \tag{21}$$

is asymptotic stable.

Proof: Select the following Lyapunov function for tracking error system **(19)**.

$$V_{1i}(t) = e_i^T(t) P_i e_i(t) \tag{22}$$

Based on an H_∞ performance bound for the closed-loop system **(19)**, one can obtain the following derivative.

$$\begin{aligned} J_i &= \dot{V}_{1i}(t) + y_i^T y_i - \gamma_i^2 f_i^T(t) f_i(t) \\ &= 2\dot{e}_i^T(t) P_i e_i(t) + + y_i^T y_i - \gamma_i^2 f_i^T(t) f_i(t) \\ &= e_i^T(t) \left(A_i^T P_i + P_i A_i - K_i^T B_i^T P_i - P_i B_i K_i\right) e_i(t) \\ &+ 2e_i^T(t) \Delta A_i^T(t) \widetilde{B}_i^T P_i e_i(t) + 2 \sum_{\substack{j\in N \\ j\neq i}} e_j^T(t) E_{ij}^T \widetilde{B}_i^T P_i e_i(t) \\ &+ 2f_i^T(t) \widetilde{B}_i^T P_i e_i(t) + e_i^T(t) C_i^T C_i e_i(t) - \gamma_i^2 f_i^T(t) f_i(t) \end{aligned} \tag{23}$$

If $\left\|\widetilde{B}_i\right\| \le b_i$ and Assumption one is satisfied, using Lemma 1, we get

$$\begin{aligned} &2e_i^T(t) \Delta A_i^T(t) \widetilde{B}_i^T P_i e_i(t) \\ &\le \varepsilon_i e_i^T(t) P_i^2 e_i(t) + \varepsilon_1^{-1} e_i^T(t) \Delta A_i^T(t) \widetilde{B}_i^T \widetilde{B}_i \Delta A_i(t) e_i(t) \\ &\le e_i^T(t) \left[\varepsilon_i P_i^2 + \varepsilon_1^{-1} a_i^2 b_i^2 I\right] e_i(t). \end{aligned} \tag{24}$$

Consider $\zeta_i^T = [e_i^T, e_{i1}^T, \cdots, e_{iN}^T, f_i^T]$ without e_{ii}^T. **Equation 23** can be rewritten as

$$\begin{aligned} J_i &= \dot{V}_{1i}(t) + y_i^T y_i - \gamma_i^2 f_i^T(t) f_i(t) \\ &= \zeta_i^T \begin{bmatrix} \Lambda_i & P_i \widetilde{B}_i E_{i1} & \cdots & P_i \widetilde{B}_i E_{iN} & P_i \widetilde{B}_i \\ * & -I & 0 & 0 & 0 \\ * & * & \ddots & 0 & 0 \\ * & * & * & -I & 0 \\ * & * & * & * & -\gamma_i^2 I \end{bmatrix} \zeta_i + \sum_{\substack{j\in N \\ j\neq i}} e_j^T e_j - e_i^T E_i e_i, \end{aligned} \tag{25}$$

where $\Lambda_i = A_i^T P_i + P_i A_i - K_i^T B_i^T P_i - P_i B_i K_i + \varepsilon_i P_i^2 + \varepsilon_1^{-1} a_i^2 b_i^2 I + C_i^T C_i + E_i$, and $E_i = \sum E_{ij}^T E_{ij}$ .The system under the equivalent control law is stable, if there is a feasible solution for the following LMI.

$$\begin{bmatrix} \Lambda_i & P_i \widetilde{B}_i E_{i1} & \cdots & P_i \widetilde{B}_i E_{iN} & P_i \widetilde{B}_i \\ * & -I & 0 & 0 & 0 \\ * & * & \ddots & 0 & 0 \\ * & * & * & -I & 0 \\ * & * & * & * & -\gamma_i^2 I \end{bmatrix} < 0 \tag{26}$$

Define $\widetilde{E}_i = (E_{i1}, \cdots, E_{iN})$, $X_i = P_i^{-1}$, and $R_i = K_i X_i$. After pre-multiplying and post-multiplying (26) by $\mathrm{diag}[X_i, I, \cdots, I]$, **Equation 26** can be rewritten as

$$\begin{bmatrix} \widetilde{\Omega}_i & \widetilde{B}_i\widetilde{E}_i & \widetilde{B}_i \\ * & -I & 0 \\ * & * & -\gamma_i^2 I \end{bmatrix} < 0, \tag{27}$$

where $\widetilde{\Omega}_i = X_i A_i^T + A_i X_i - B_i R_i - R_i^T B_i^T + \varepsilon_i I + \varepsilon_i^{-1} a_i^2 b_i^2 X_i^2 + X_i C_i^T C_i X_i + X_i E_i X_i$. Then, the LMI **(20)** is obtained with the method of Lemma three and the proof is completed.In the following section, we design the switching control in terms of adaptive algorithm to restrain the state chattering.

Theorem 2: Design the following controller **(28)** for closed-loop system **(11)** in terms of the feasible solution obtained via **(20)** and the system dynamic is asymptotic stable based on

$$u_i(t) = -K_i e_i(t) - \widetilde{H}_i \widehat{a}_i(t) e_i(t) - \widetilde{H}_i \sum_{\substack{j\in N \\ j\neq i}} E_{ij} e_j(t) - \widehat{\rho}_i(t)\widetilde{H}_i \frac{H_i^T s_i(t)}{\left\| s_i^T(t) H_i \right\|} \tag{28}$$

where $\widetilde{H}_i = (H_i B_i)^{-1} H_i$ and the adaptive laws are

$$\dot{\widehat{a}}_i(t) = q_{i1} s_i^T(t) H_i e_i(t) \tag{29}$$

$$\dot{\widehat{\rho}}_i(t) = q_{i2} \left\| s_i^T(t) H_i \right\| \tag{30}$$

where q_{i1} and q_{i2} are positive parameters.

Proof: Let us consider the following Lyapunov function:

$$V_{2i}(t) = \frac{1}{2} s_i^T(t) s_i(t) + \frac{1}{2q_{i1}} \widetilde{a}_i^2(t) + \frac{1}{2q_{i2}} \widetilde{\rho}_i^2(t) \tag{31}$$

where $\widetilde{a}_i(t) = a_i - \widehat{a}_i(t)$, and $\widetilde{\rho}_i(t) = \rho_i - \widehat{\rho}_i(t)$. Based on **(28)**, **(29)** and **(30)**, its derivative is given by

$$\begin{aligned} \dot{V}_{2i}(t) &= s_i^T(t)\dot{s}_i(t) + \frac{1}{q_{i1}}\widetilde{a}_i(t)\left(-\dot{\widehat{a}}_i(t)\right) + \frac{1}{q_{i2}}\widetilde{\rho}_i(t)\left(-\dot{\widehat{\rho}}_i(t)\right) \\ &= s_i^T(t)\left(H_i\dot{e}_i(t) - H_i(A_i - B_iK_i)e_i(t)\right) \\ &-\widetilde{a}_i(t) s_i^T(t) H_i e_i(t) - \widetilde{\rho}_i(t)\left\| s_i^T(t) H_i \right\| \\ &= s_i^T(t) H_i \Delta A_i(t) e_i(t) - s_i^T(t) H_i \widehat{a}_i(t) e_i(t) \\ &+ s_i^T(t) H_i f_i(t) - \rho_i(t) s_i^T(t) H_i \frac{H_i^T s_i(t)}{\left\| s_i^T(t) H_i \right\|} \\ &-\widetilde{a}_i(t) s_i^T(t) H_i e_i(t) - \widetilde{\rho}_i(t)\left\| s_i^T(t) H_i \right\| \\ &= s_i^T(t) H_i \Delta A_i(t) e_i(t) - a_i s_i^T(t) H_i e_i(t) \\ &+ s_i^T(t) H_i f_i(t) - \rho_i \left\| s_i^T(t) H_i \right\| \\ &\le \left\| \Delta A_i(t) \right\| \left\| s_i^T(t) H_i e_i(t) \right\| - a_i s_i^T(t) H_i e_i(t) \\ &+ \left\| f_i(t) \right\| \left\| s_i^T(t) H_i \right\| - \rho_i \left\| s_i^T(t) H_i \right\| \le 0 \end{aligned} \tag{32}$$

Obviously, the derivative of the Lyapunov function $V_{2i}(t) \le 0$ is verified. That means the system states will reach the designed sliding mode surface in finite time for arbitrary $s_i(t) \neq 0$. Then, the proof is completed.

SIMULATION RESULTS

In this section, the proposed decentralized ASMC strategy is applied in the voltage control of microgrid with ring topology. The microgrid on study contains four DGus ($N = 4$) and the nominal frequency is 60Hz, that means $\omega_0 = 120\pi rad/s$. The electrical parameters of the subsystems and interconnecting lines are concluded in **Table 1** and **Table 2**, respectively.

The intermittence of the renewable generation and the uncertaintiy of the local load in microgrid will influence the power sharing among subsystems and cause frequency fluctuation indirectly. In this case, we consider the frequency fluctuation $\Delta\omega = \sin(1000\pi t)$, the current generated by DGu in subsystem one is increased by 20% at $t = 1$s and recover to the original state at $t = 2$s. Furthermore, the current generated by DGu in subsystem three is reduced by 50% at $t = 1$s and recover to the original state at $t = 2$s. On the contrary, the operation states in subsystem two and four are constant. In order to ensure the power sharing, the voltages of PCCs and currents of interconnecting lines should also change. The reference values of voltages and currents in each subsystem are expressed in **Table 3**.

In the following simulation procedures, we analysis the simulation results and verify the validity of the proposed decentralized ASMC strategies under frequency disturbances and local load uncertainties. Because the system uncertainties are bounded, we can get $a_i \ge 1$, $b_i = 1.7321$. The initial states are $e_1(0) = [5\ -32\ -0.2\ \ 1.5\ \ 1.5]^T$, $e_2(0) = [4.5\ -3.1\ 4\ -0.1\ 1.5\ 2]^T$, $e_3(0) = [4.4\ -3.2\ 1.7\ -0.1\ 2.5\ 1.7]^T$ and $e_4(0) = [4.3\ 3.5\ 3.2\ -0.2\ 1.8\ 2.6]^T$. According to Theroem 1, a couple of feasible solutions can be obtained as follows,

$$H_1 = \begin{bmatrix} 0.0095 & 0 & 0.0095 & 0 & 0.0095 & 0 \\ 0 & 0.0095 & 0 & 0.0095 & 0 & 0.0095 \end{bmatrix},$$

$$H_2 = \begin{bmatrix} 0.0092 & 0 & 0.0092 & 0 & 0.0092 & 0 \\ 0 & 0.0092 & 0 & 0.0092 & 0 & 0.0092 \end{bmatrix},$$

$$H_3 = \begin{bmatrix} 0.0087 & 0 & 0.0087 & 0 & 0.0087 & 0 \\ 0 & 0.0087 & 0 & 0.0087 & 0 & 0.0087 \end{bmatrix},$$

$$H_4 = \begin{bmatrix} 0.0083 & 0 & 0.0083 & 0 & 0.0083 & 0 \\ 0 & 0.0083 & 0 & 0.0083 & 0 & 0.0083 \end{bmatrix},$$

$$K_1 = \begin{bmatrix} 9214.5902 & 0 & 2416.5281 & 0 & -6560.1562 & 0 \\ 0 & 9214.5902 & 0 & 2416.5281 & 0 & -6560.1562 \end{bmatrix},$$

$$K_2 = \begin{bmatrix} 8795.6529 & 0 & 2451.4103 & 0 & -8789.3652 & 0 \\ 0 & 8795.6529 & 0 & 2451.4103 & 0 & -8789.3652 \end{bmatrix},$$

$$K_3 = \begin{bmatrix} 10225.614 & 0 & 2484.2629 & 0 & -12448.709 & 0 \\ 0 & 10225.614 & 0 & 2484.2629 & 0 & -12448.709 \end{bmatrix},$$

$$K_4 = \begin{bmatrix} 8079.6892 & 0 & 2208.2329 & 0 & 5562.70592 & 0 \\ 0 & 8079.6892 & 0 & 2208.2329 & 0 & 5562.70592 \end{bmatrix}.$$

In order to restrain the mismatched uncertainties and external disturbances, for tracking error system **(11)**, the adaptive parameters are selected as

$$q_{11} = 1.2,\ q_{21} = 0.9,\ q_{31} = 1.1,\ q_{41} = 1.5$$

TABLE 1 | Electrical parameters of the microgrid.

Subsystems	Filter parameters		Capacitance
	R_{ti} (mΩ)	L_{ti} (mH)	C_{ti} (μF)
Subsystem 1	40.2	9.5	62.86
Subsystem 2	38.7	9.2	62.86
Subsystem 3	34.6	8.7	62.86
Subsystem 4	31.8	8.3	62.86

TABLE 2 | Electrical parameters of the interconnecting lines.

Line impedance Z_i	R_i (Ω)	L_i (mH)
Line 1	7.6	111.9
Line 2	8	140
Line 3	7.3	165
Line 4	7.8	190

TABLE 3 | The reference values of state variables in each subsystem.

Time(s)	Subsystem1				Subsystem2			
	Voltages (V)		Currents (A)		Voltages (V)		Currents (A)	
	V^*_{d1}	V^*_{q1}	I^*_{td1}	I^*_{tq1}	V^*_{d2}	V^*_{q2}	I^*_{td2}	I^*_{tq2}
0–1	390	−0.5	50.2	−10.6	370	−1	100.1	−6.8
1–2	385	−0.5	70.2	−10.6	370	−1	100.1	−6.8
2–3	390	−0.5	50.2	−10.6	370	−1	100.1	−6.8
Time(s)	**Subsystem3**				**Subsystem4**			
	Voltages (V)		Currents (A)		Voltages (V)		Currents (A)	
	V^*_{d3}	V^*_{q3}	I^*_{td3}	I^*_{tq3}	V^*_{d4}	V^*_{q4}	I^*_{td4}	I^*_{tq4}
0–1	360	−0.6	40.1	−1.8	350	−1	80.1	−10.4
1–2	365	−0.6	20.1	−1.8	350	−1	80.1	−10.4
2–3	360	−0.6	40.1	−1.8	350	−1	80.1	−10.4

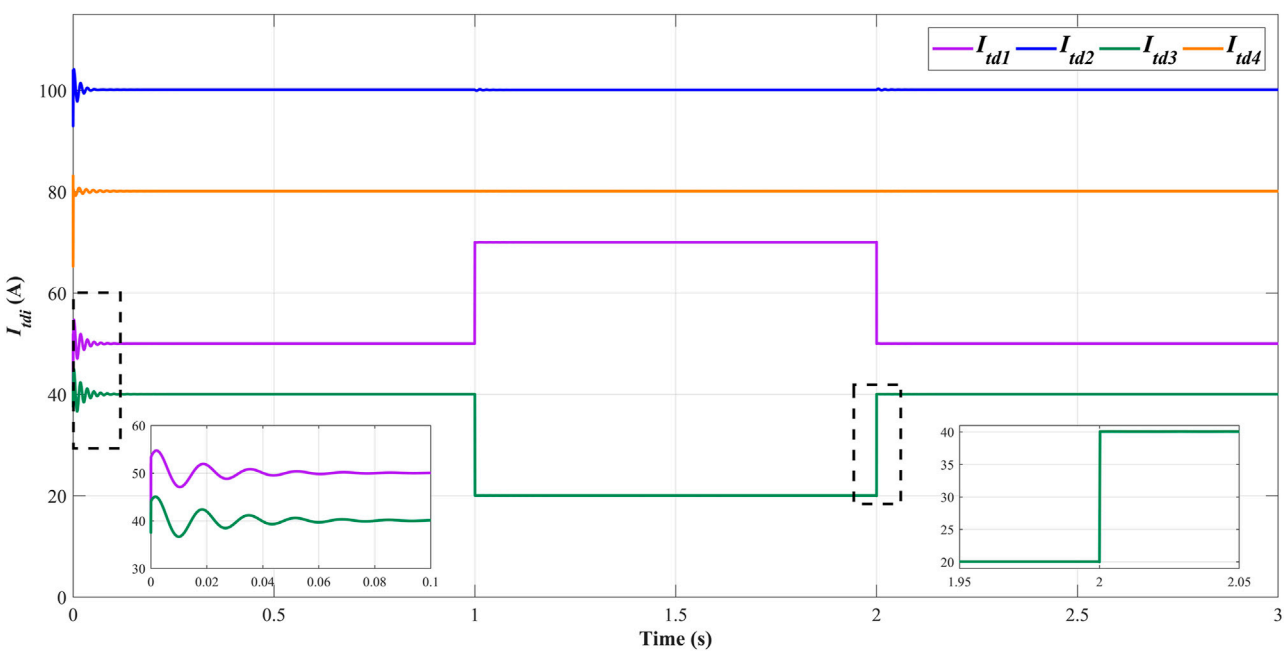

FIGURE 2 | Time evolution of the *d*-component of currents generated from DGus.

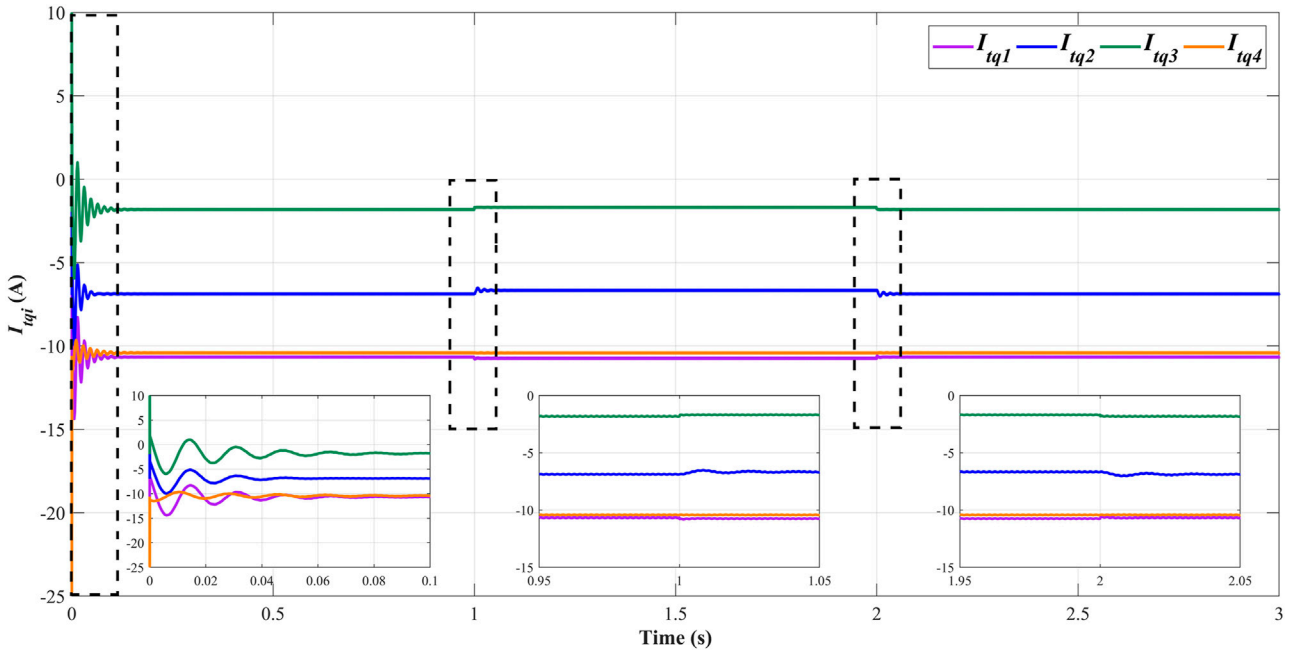

FIGURE 3 | Time evolution of the *q*-component of currents generated from DGus.

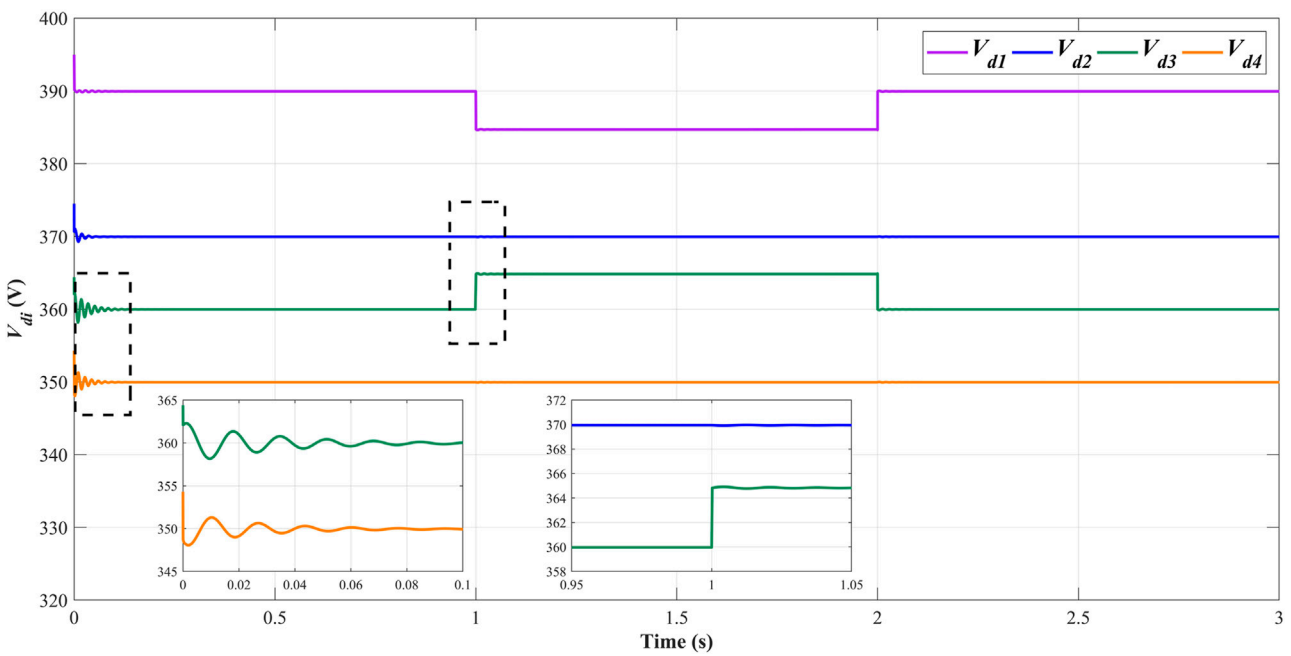

FIGURE 4 | Time evolution of the *d*-component of voltages of PCCs.

$$q_{12} = 1.0,\ q_{22} = 3.2,\ q_{32} = 3.7,\ q_{42} = 5.74$$

The voltages and currents of the islanded microgrid demonstrate superior robustness and tracking error performance under the proposed decentralized ASMC strategy. The time evolutions of the *dq*-components of the currents generated from each DGu are depicted in **Figure 2** and **Figure 3** respectively in the case of load currents mutation. I_{ld1} increases 20 A at $t = 1$s and I_{td1} increases 20 A synchronously, while I_{tq1} does not change significantly. Similarly, the current generated from DGu3 varies with the local load current in subsystem 3, and the current dynamic

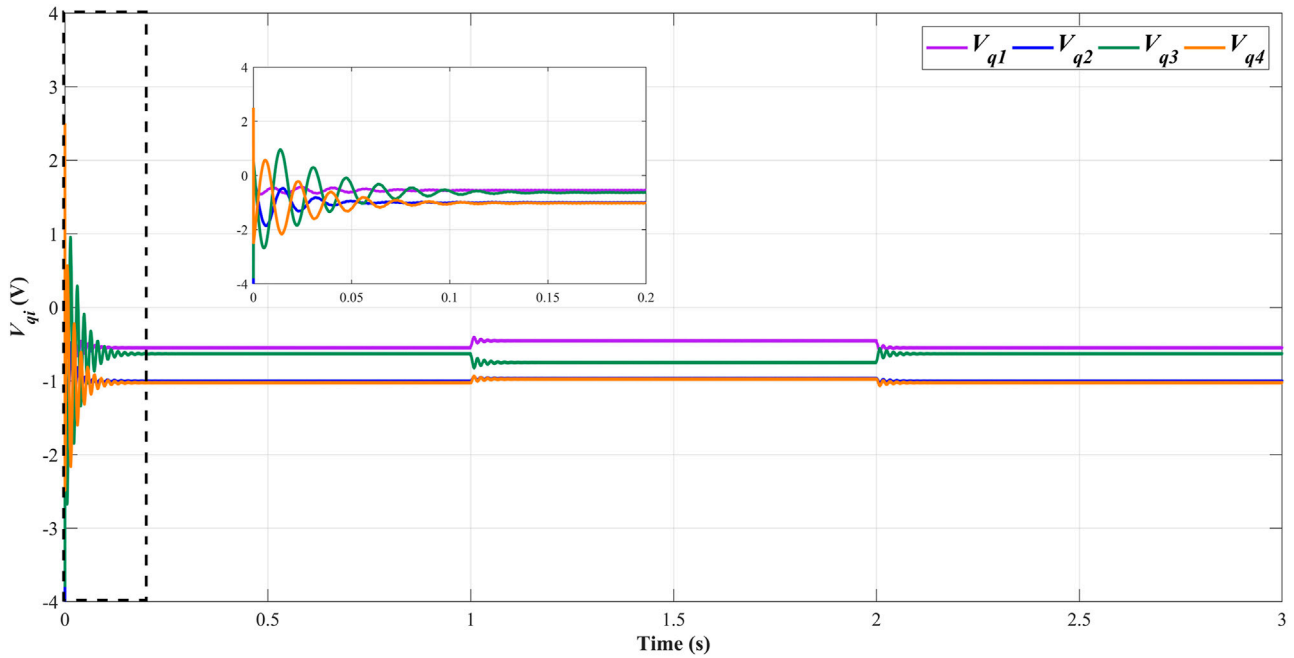

FIGURE 5 | Time evolution of the *q*-component of voltages of PCCs.

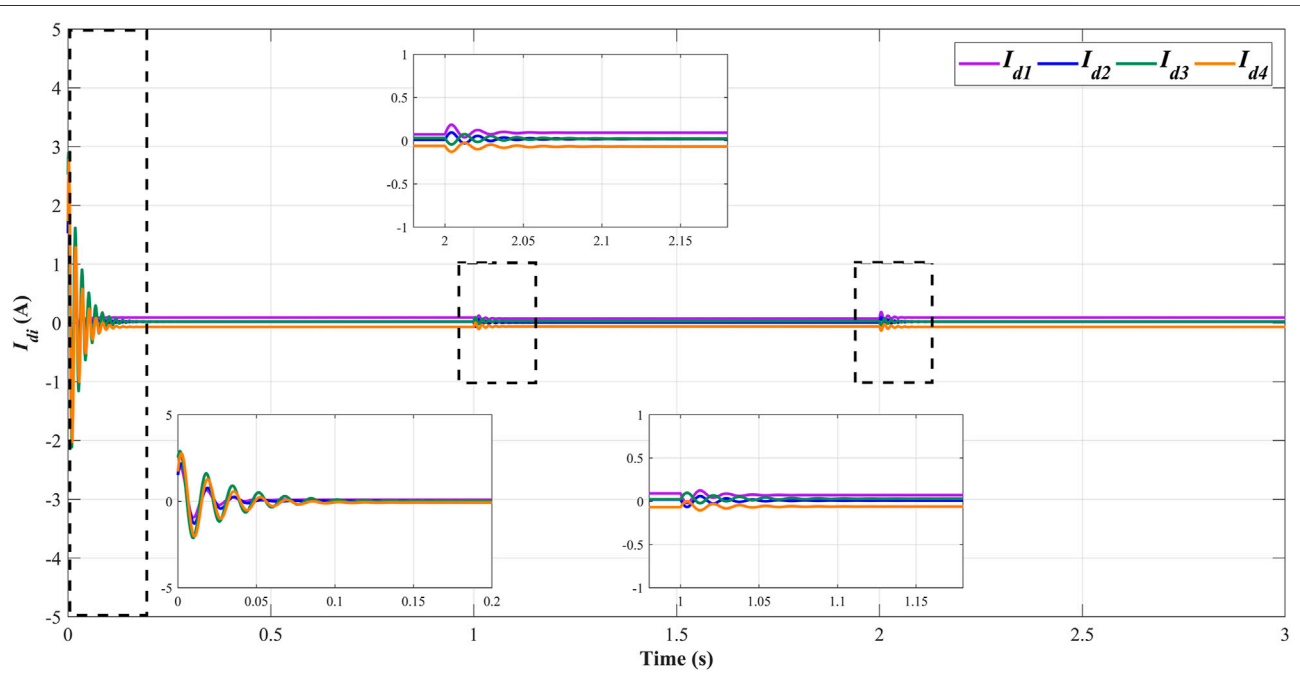

FIGURE 6 | Time evolution of the *d*-component of currents of interconnecting lines.

curves illustrate excellent robustness when local load current mutates.

The time evolutions of the *dq*-components of the PCC voltages of each subsystem are shown in **Figure 4** and **Figure 5**. Considering the load current variations in the interconnected microgrid system, V_{d1} is decreased by 5 V and V_{d3} is increased by 5 V. Meanwhile, I_{d1} provided by subsystem one is reduced and I_{d3} provided to subsystem four is improved. Then, the power sharing among each subsystem can be ensured. As shown in **Figure 4**, there exist deviations between initial voltage values and nominal values, but the system voltages can also track to the nominal values and maintain stable. When the *d*-components of the

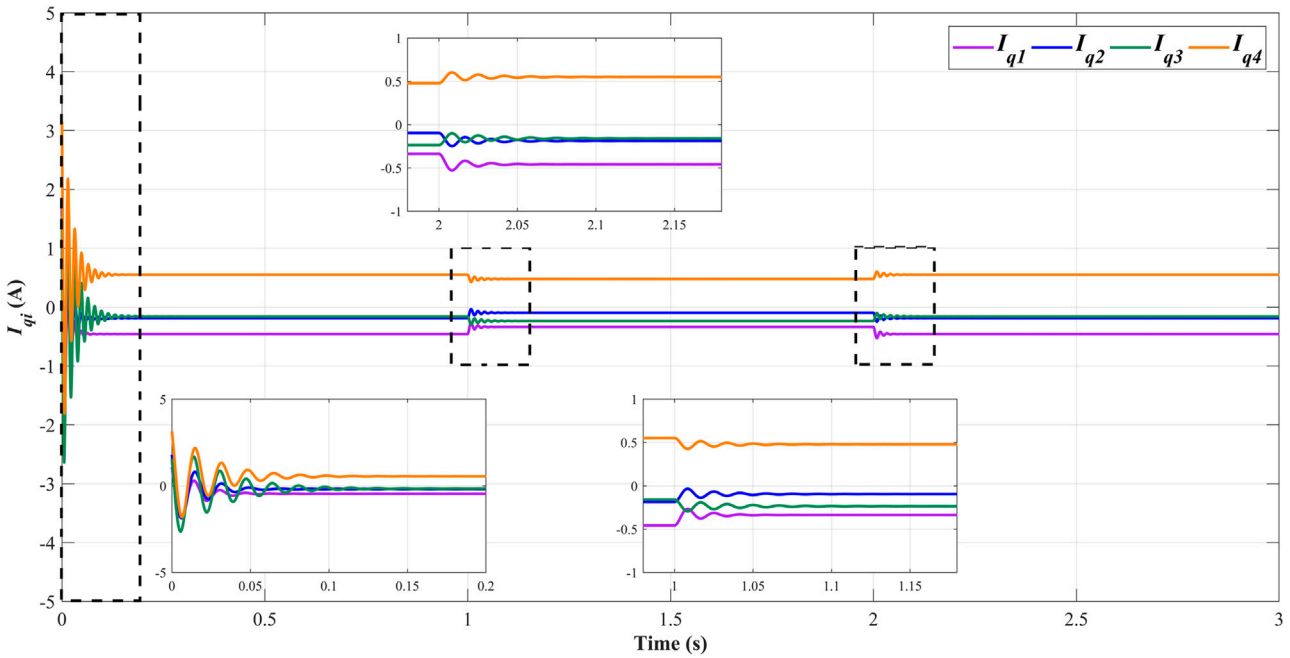

FIGURE 7 | Time evolution of the *q*-component of currents of interconnecting lines.

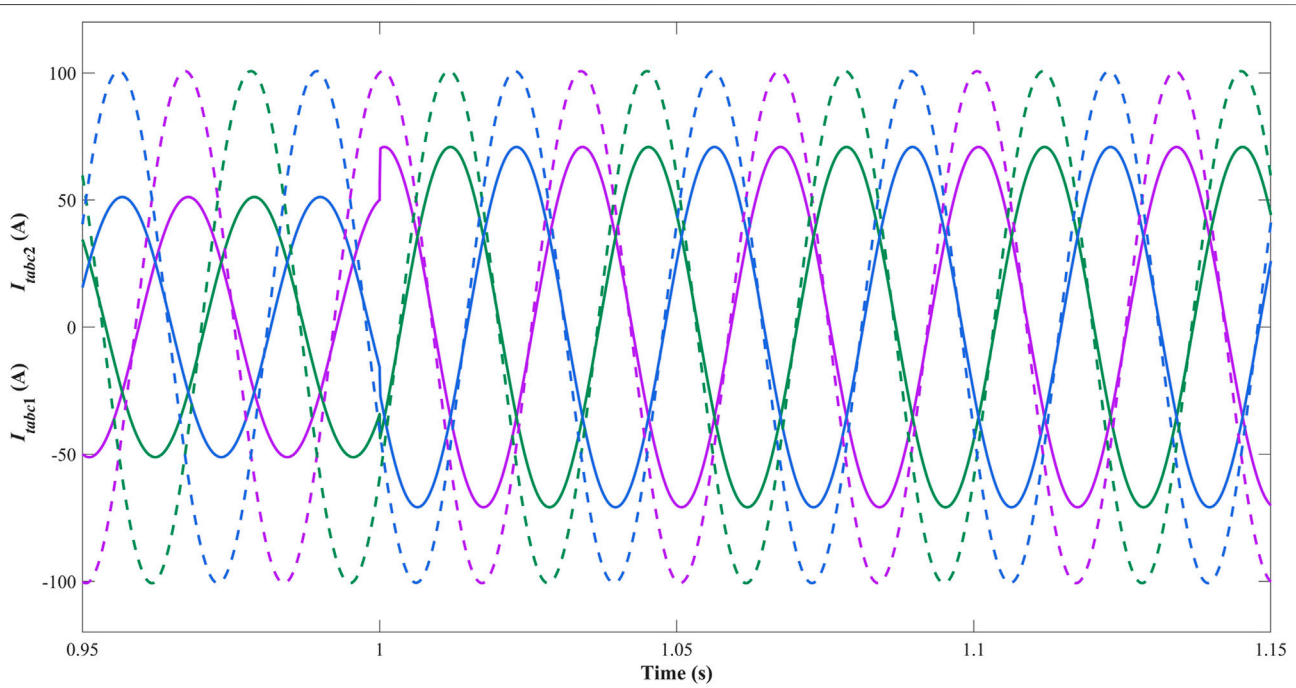

FIGURE 8 | Three-phase waveforms of currents generated from DGu1 and DGu2.

voltages change in small scales, the *q*-components of the voltages fluctuate and remain stable in a short time.

The time evolutions of the *dq*-components of the currents of interconnecting lines are represented in **Figure 6** and **Figure 7**. Under the influence of mutations of load currents and PCC voltages, the currents of interconnecting lines are only influenced by the voltages of PCCs and do not deviate from the reference values appreciably, which illustrates the remarkable robustness of proposed ASMC strategy against the external disturbances and mismatched uncertainties. That also means the changes of local

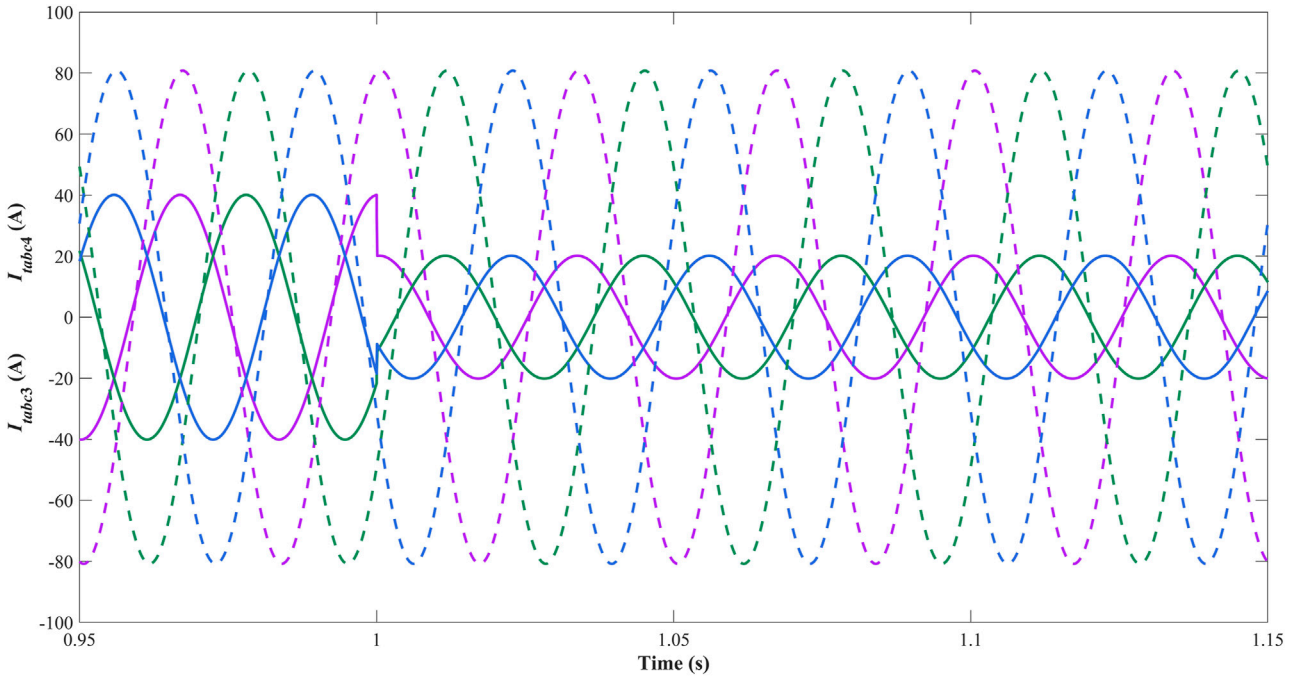

FIGURE 9 | Three-phase waveforms of currents generated from DGu3 and DGu4.

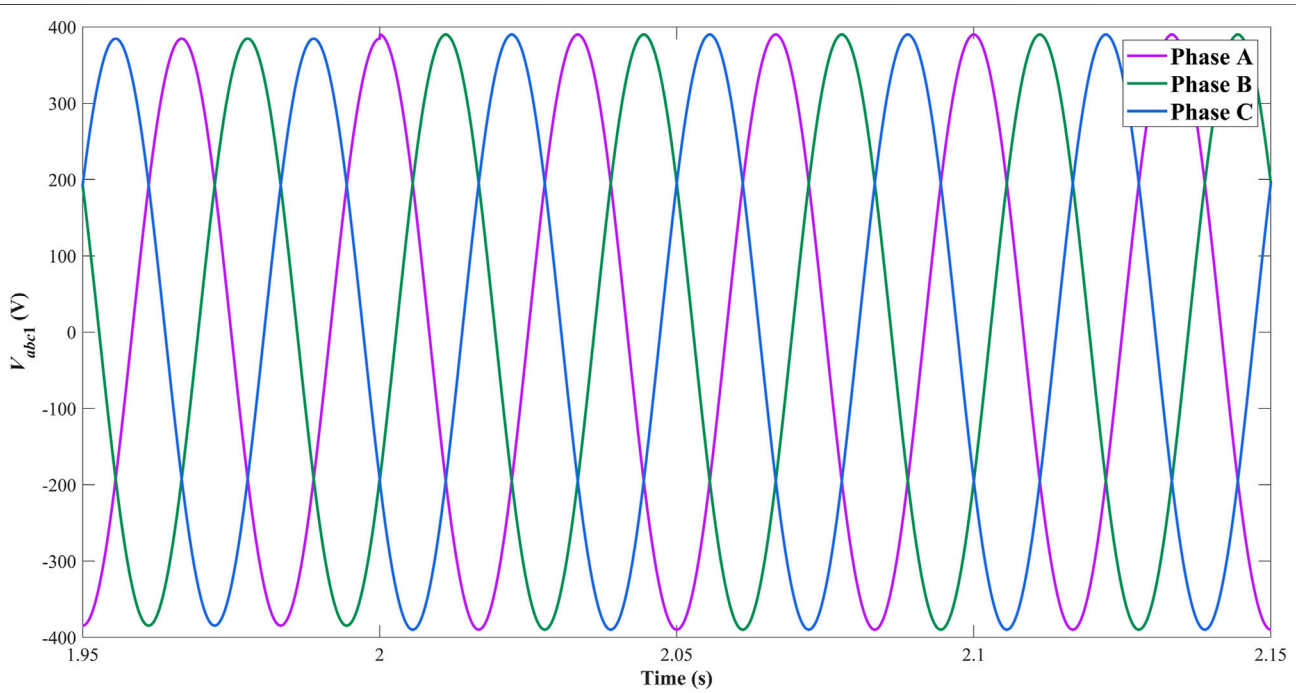

FIGURE 10 | Three-phase waveforms of PCC1 voltage.

load currents will not influence the stability of the general microgrid. Notably, the current orientation of line four is opposite compared with the currents of other lines because the voltage of PCC four is lower than that of PCC1.

Figure 8 and **Figure 9** depict the three-phase waveforms of currents generated from DGus. **Figure 10** and **Figure 11** depict the three-phase waveforms of voltages of PCCs in subsystem one and subsystem 3. In islanded mode, the decentralized controllers are

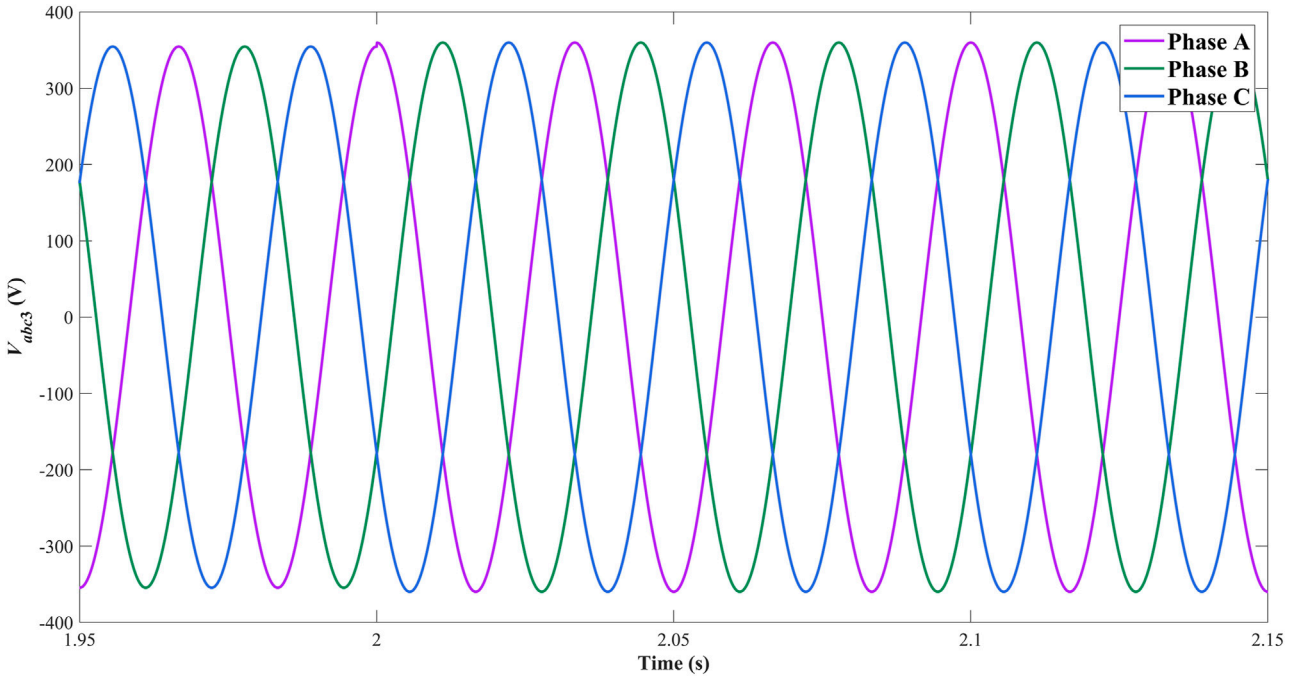

FIGURE 11 | Three-phase waveforms of PCC3 voltage.

mainly designed to standardize the voltage and current waves and improve the power quality of AC microgrid. In **Figure 8** and **Figure 9**, the amplitude of three-phase wave of the current generated from DGu1 increases 20 A and that of DGu3 decreases 20 A at $t = 1$s, which matches with the variations of load currents. In **Figure 10** and **Figure 11**, it is obvious that the three-phase waves of the voltages of PCC1 and PCC3 maintain in standard waveform and the effectiveness and reliability can be proved adequately.

CONCLUSION

In this paper, the chattering restraint issues for voltage control of the islanded microgrid with a ring topology structure have been solved via decentralized adaptive sliding mode control strategies. The constructed tracking error system with interconnections has depicted the interaction among each subsystem appropriately. The control matrices in sliding mode surfaces have been obtained via solving the LMIs, which combine the H_∞ attenuation performance of the system external disturbances with the asymptotic stabilities of integral sliding mode surfaces. The controller parameters have been optimized by means of adaptive algorithms. The simulation results have illustrated the effectiveness of the proposed decentralized ASMC strategies. In future, further research will be extended to the nonlinear and time-delay system.

DATA AVAILABILITY STATEMENT

The raw data supporting the conclusions of this article will be made available by the authors, without undue reservation.

AUTHOR CONTRIBUTIONS

HJ was responsible for the main idea and writing work of this paper. YZ and JH were responsible for the mathematical derivation. MW was responsible for the simulation part.

FUNDING

Doctoral Scientific Research Foundation of Liaoning Province (2020-BS-181). Liaoning Revitalization Talents Program (XLYC1907138). Natural Science Foundation of Liaoning Province (2019-MS-239). Key R&D Program of Liaoning Province (2020JH2/10300101).

REFERENCES

Avelar, H. J., Parreira, W. A., Vieira, J. B., de Freitas, L. C. G., and Coelho, E. A. A. (2012). A State Equation Model of a Single-phase Grid-Connected Inverter Using a Droop Control Scheme with Extra Phase Shift Control Action. *IEEE Trans. Ind. Electron.* 59, 1527–1537. doi:10.1109/TIE.2011.2163372

Beerten, J., and Belmans, R. (2013). Analysis of Power Sharing and Voltage Deviations in Droop-Controlled DC Grids. *IEEE Trans. Power Syst.* 28, 4588–4597. doi:10.1109/TPWRS.2013.2272494

Chen, Z., Luo, A., Wang, H., Chen, Y., Li, M., and Huang, Y. (2015). Adaptive Sliding-Mode Voltage Control for Inverter Operating in Islanded Mode in Microgrid. *Int. J. Electr. Power Energ. Syst.* 66, 133–143. doi:10.1016/j.ijepes.2014.10.054

Cucuzzella, M., Incremona, G. P., and Ferrara, A. (2017). Decentralized Sliding Mode Control of Islanded AC Microgrids with Arbitrary Topology. *IEEE Trans. Ind. Electron.* 64, 6706–6713. doi:10.1109/TIE.2017.2694346

Divshali, P. H., Alimardani, A., Hosseinian, S. H., and Abedi, M. (2012). Decentralized Cooperative Control Strategy of Microsources for Stabilizing Autonomous VSC-Based Microgrids. *IEEE Trans. Power Syst.* 27, 1949–1959. doi:10.1109/TPWRS.2012.2188914

Eren, S., Pahlevani, M., Bakhshai, A., and Jain, P. (2015). An Adaptive Droop DC-Bus Voltage Controller for a Grid-Connected Voltage Source Inverter with LCL Filter. *IEEE Trans. Power Electron.* 30, 547–560. doi:10.1109/TPEL.2014.2308251

Esparza, M., Segundo, J., Nunez, C., Wang, X., and Blaabjerg, F. (2017). A Comprehensive Design Approach of Power Electronic-Based Distributed Generation Units Focused on Power-Quality Improvement. *IEEE Trans. Power Deliv.* 32, 942–950. doi:10.1109/TPWRD.2016.2584616

Hu, J., Nian, H., Hu, B., He, Y., and Zhu, Z. Q. (2010). Direct Active and Reactive Power Regulation of DFIG Using Sliding-Mode Control Approach. *IEEE Trans. Energ. Convers.* 25, 1028–1039. doi:10.1109/TEC.2010.2048754

Kabalan, M., Singh, P., and Niebur, D. (2017). Large Signal Lyapunov-Based Stability Studies in Microgrids: A Review. *IEEE Trans. Smart Grid* 8, 2287–2295. doi:10.1109/TSG.2016.2521652

Karimi, H., Davison, E. J., and Iravani, R. (2010). Multivariable Servomechanism Controller for Autonomous Operation of a Distributed Generation Unit: Design and Performance Evaluation. *IEEE Trans. Power Syst.* 25, 853–865. doi:10.1109/TPWRS.2009.2031441

Liu, J., Gao, Y., Luo, W., and Wu, L. (2017). Takagi-Sugeno Fuzzy-Model-Based Control of Three-Phase AC/DC Voltage Source Converters Using Adaptive Sliding Mode Technique. *IET Control. Theor. Appl.* 11, 1255–1263. doi:10.1049/iet-cta.2016.0689

Mahmoud, M. S., Azher Hussain, S., and Abido, M. A. (2014). Modeling and Control of Microgrid: An Overview. *J. Franklin Inst.* 351, 2822–2859. doi:10.1016/j.jfranklin.2014.01.016

Mi, Y., Song, Y., Fu, Y., and Wang, C. (2020). The Adaptive Sliding Mode Reactive Power Control Strategy for Wind-Diesel Power System Based on Sliding Mode Observer. *IEEE Trans. Sustain. Energ.* 11, 2241–2251. doi:10.1109/TSTE.2019.2952142

Mi, Y., Zhang, H., Fu, Y., Wang, C., Loh, P. C., and Wang, P. (2019). Intelligent Power Sharing of DC Isolated Microgrid Based on Fuzzy Sliding Mode Droop Control. *IEEE Trans. Smart Grid* 10, 2396–2406. doi:10.1109/TSG.2018.2797127

Mnasri, C., and Gasmi, M. (2011). LMI-Based Adaptive Fuzzy Integral Sliding Mode Control of Mismatched Uncertain Systems. *Int. J. Appl. Maths. Comput. Sci.* 21, 605–615. doi:10.2478/v10006-011-0047-5

Rui, W., Qiuye, S., Dazhong, M., and Xuguang, H. (2020). Line Impedance Cooperative Stability Region Identification Method for Grid-Tied Inverters under Weak Grids. *IEEE Trans. Smart Grid* 11, 2856–2866. doi:10.1109/TSG.2020.2970174

Sahoo, S. K., Sinha, A. K., and Kishore, N. K. (2018). Control Techniques in AC, DC, and Hybrid AC-DC Microgrid: A Review. *IEEE J. Emerg. Sel. Top. Power Electron.* 6, 738–759. doi:10.1109/JESTPE.2017.2786588

Sefa, I., Altin, N., Ozdemir, S., and Kaplan, O. (2015). Fuzzy PI Controlled Inverter for Grid Interactive Renewable Energy Systems. *IET Renew. Power Generation* 9, 729–738. doi:10.1049/iet-rpg.2014.0404

Vandoorn, T. L., Ionescu, C. M., De Kooning, J. D. M., De Keyser, R., and Vandevelde, L. (2013). Theoretical Analysis and Experimental Validation of Single-Phase Direct Versus Cascade Voltage Control in Islanded Microgrids. *IEEE Trans. Ind. Electron.* 60, 789–798. doi:10.1109/TIE.2012.2205362

Wang, R., Sun, Q., Hu, W., Li, Y., Ma, D., and Wang, P. (2021). SoC-Based Droop Coefficients Stability Region Analysis of the Battery for Stand-Alone Supply Systems with Constant Power Loads. *IEEE Trans. Power Electron.* 36, 7866–7879. doi:10.1109/TPEL.2021.3049241

Wang, R., Sun, Q., Ma, D., and Liu, Z. (2019). The Small-Signal Stability Analysis of the Droop-Controlled Converter in Electromagnetic Timescale. *IEEE Trans. Sustain. Energ.* 10, 1459–1469. doi:10.1109/TSTE.2019.2894633

Zeb, K., Islam, S. U., Din, W. U., Khan, I., Ishfaq, M., Busarello, T. D. C., et al. (2019). Design of Fuzzy-PI and Fuzzy-Sliding Mode Controllers for Single-Phase Two-Stages Grid-Connected Transformerless Photovoltaic Inverter. *Electronics* 8, 520–539. doi:10.3390/electronics8050520

Zhou, B., Zou, J., Yung Chung, C., Wang, H., Liu, N., Voropai, N., et al. (2021). Multi-Microgrid Energy Management Systems: Architecture, Communication, and Scheduling Strategies. *J. Mod. Power Syst. Clean Energ.* 9, 463–476. doi:10.35833/MPCE.2019.000237

Zou, H., Mao, S., Wang, Y., Zhang, F., Chen, X., and Cheng, L. (2019). A Survey of Energy Management in Interconnected Multi-Microgrids. *IEEE Access* 7, 72158–72169. doi:10.1109/ACCESS.2019.2920008

Conflict of Interest: The authors declare that the research was conducted in the absence of any commercial or financial relationships that could be construed as a potential conflict of interest.